

EQUILIBRIUM AND STABILITY OF A CIRCULARLY  
TOWED CABLE SUBJECT TO AERODYNAMIC DRAG

J. J. Russell\*

Associate Professor of Engineering Mechanics  
Department of Civil Engineering, Engineering Mechanics and Materials  
United States Air Force Academy  
Colorado

W. J. Anderson\*

Professor of Aerospace Engineering  
Department of Aerospace Engineering  
The University of Michigan  
Ann Arbor, Michigan

Abstract

The finite element method is used to study the equilibrium and stability of an elastic cable whose upper end is towed in a horizontal, circular path at a constant angular velocity. Fluid drag is assumed to be composed of tangential and normal components which are proportional to the tangential and normal velocity components squared, respectively. The problem includes strong geometric nonlinearities and is nonconservative, thereby admitting both static and dynamic instabilities.

Equilibrium equations for a cable element including elastogeometric, centripetal, and aerodynamic stiffness matrices are developed in terms of problem parameters and a shape function. All geometric nonlinearities are retained, but small elongations are assumed. The resulting nonlinear algebraic equations are solved using a Newton-Raphson procedure. The stability of an equilibrium position is determined by perturbing the nonlinear equations of motion and calculating the eigenvalues of the resulting linearized dynamic equations.

Results indicate multivalued solutions, the number depending on the rotational frequency and tow radius. Both static "jump" type and dynamic instabilities are found.

I. Introduction

While no practical interest has been shown until the last two decades, the equilibrium configuration of a cable towed in a circular path has been of theoretical interest since antiquity. Solutions to the "linearized" eigenvalue problem (zero tow radius) were obtained first by D. Bernoulli (1700-1782) and L. Euler (1707-1783). Work then ceased for two hundred years until Kolodner's study<sup>(1)</sup> on the nature of the nonlinear eigenvalue problem. Asymptotic solutions for high rotational frequencies were considered by Wu<sup>(2)</sup>. Caughey<sup>(3)</sup> was the first to analyze the nonlinear forced response (nonzero tow radius) and note the similarity of the response to that of a hardening spring-mass system. All authors thus far had considered the towing medium to be a vacuum.

Nate Saint, a missionary working in South America, motivated practical interest in the circularly towed cable idea as a possible aerial delivery system by demonstrating in the early 1950's that a light, fixed-wing aircraft could be used to deliver food and medical supplies to remote villages. He accomplished this by towing a cable with a basket attached to the end from an aircraft orbiting over the delivery point. Surprisingly, the basket hovered almost motionlessly near the ground.

Since then, many researchers have studied the problem, introducing new solution techniques and applications. Skop and Choo<sup>(4)</sup> and Crist<sup>(5)</sup> considered the equilibrium configuration for the case of aerodynamic drag, Skop and Choo being the first to demonstrate the multisolution nature of the problem. Crist<sup>(6)</sup> studied the effects of crosswind and the transient problems associated with towing the cable into and out of orbit from a rectilinear path. Huang<sup>(7)</sup> also restricted his work to the airborne system but was primarily interested in maximizing the cable verticality. The towing medium was changed from air to water when Choo<sup>(8)</sup> considered marine applications.

The finite element method is an extremely powerful approach for problems of this type since it has the advantages of structural assembly, equivalent nodal load creation, ease of modification, and boundary condition application. The present paper seeks to extend the work of the authors<sup>(9)</sup> which employed a linear element to study the circularly towed cable subject to viscous drag to one subject to aerodynamic drag. Webster<sup>(10)</sup> has since independently developed a linear cable element, while Henghold and Russell<sup>(11)</sup> have developed a complete family of higher order cable elements.

The equilibrium equations referred to the rotating coordinate system and perturbed equations for small motion about the equilibrium point are developed now for a single element using the principle of virtual work.

\* Member AIAA, Associate Member ASME  
\*\* Member AIAA

## II. Element Equilibrium

An elastic cable of undeformed length  $l$  and mass per unit length  $m$ , with its upper end rotated about the Z axis at a constant angular velocity  $\omega$  is shown in Fig. 1. The  $\bar{X}\bar{Y}\bar{Z}$  system is an inertial reference frame while the XYZ system rotates with the tow point. The final deformed length of the cable is  $l^*$ .

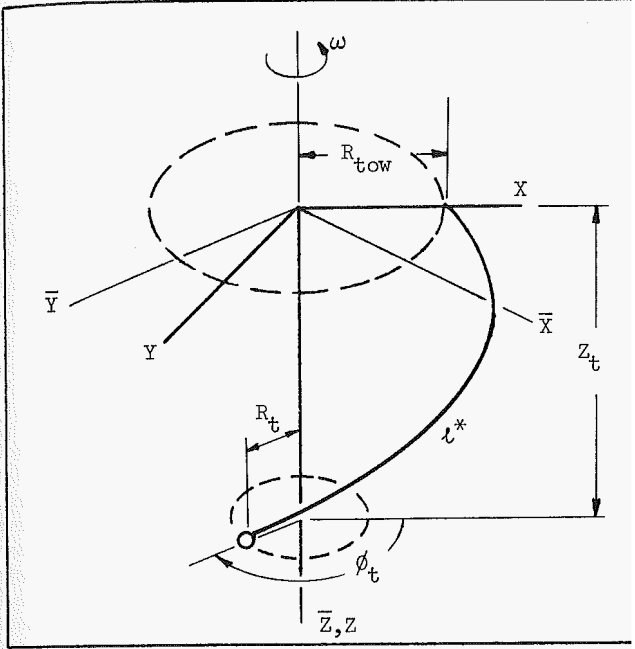


Figure 1. The Cable Configuration

The location of any material coordinate in the deformed geometry is

$$\{X^*\} = \{X^*(S)\} \quad (1)$$

where  $\{X^*\} = \{X^*Y^*Z^*\}^T$  and  $S$  is the undeformed arc length. The velocity  $\{v^*\}$  and acceleration  $\{a^*\}$  can be written in matrix form as

$$\{v^*\} = [a_I] \{\dot{X}^*\} + \omega [a_G] \{X^*\} \quad (a)$$

$$\{a^*\} = [a_I] \{\ddot{X}^*\} + 2\omega [a_G] \{\dot{X}^*\} - \omega^2 [a_C] \{X^*\} \quad (b)$$

where  $(\dot{\quad})$  indicates differentiation with respect to time and the following matrices have been defined

$$[a_I] = \begin{bmatrix} 1 & 0 & 0 \\ 0 & 1 & 0 \\ 0 & 0 & 1 \end{bmatrix} \quad [a_G] = \begin{bmatrix} 0 & 1 & 0 \\ -1 & 0 & 0 \\ 0 & 0 & c \end{bmatrix} \quad [a_C] = \begin{bmatrix} 1 & 0 & 0 \\ 0 & 1 & 0 \\ 0 & 0 & 0 \end{bmatrix} \quad (3)$$

Applying the principle of virtual work to a cable element of undeformed arc length  $L$  and deformed arc length  $L^*$  yields

$$\delta W = \int_{L^*} \{\delta X^*\}^T \{f^*\} dS^* + \{\delta X_N^*\}^T \{r^*\} -$$

$o$

$$\int A \sigma_s \delta \epsilon_s dS = 0 \quad (4)$$

$o$

where the following terms have been used:

$\epsilon_s$ , the Lagrangian strain in the deformed axial direction

$$\epsilon_s = \frac{1}{2} [(\bar{\partial} S^*)^2 - 1] \quad (5)$$

$\sigma_s$ , the Kirchoff stress which is related to  $\epsilon_s$  through the modulus of elasticity  $E$  for a linearly elastic material by

$$\sigma_s = E \epsilon_s \quad (6)$$

$A$ , the undeformed cable cross-sectional area

$\{f^*\}$ , the distributed load per unit deformed arc length,

$\{X_N^*\}$ , the nodal coordinates and

$\{r^*\}$ , the corresponding nodal load vector.

The shape function  $[N]$  relating the coordinates of a generic point to the nodal coordinates is then given by

$$\{X^*\} = [N] \{X_N^*\} \quad (7)$$

Using the shape function definition (7), as well as the definitions of  $\epsilon_s$  (5) and  $\sigma_s$  (6) allows the internal virtual work expression  $\delta U$  to be written in terms of the shape function and nodal coordinates.

$$\delta U = \{\delta X_N^*\}^T \left[ \frac{1}{2} \int_0^L A E (\{X_N^*\}^T [N']^T [N'] \{X_N^*\} - 1) [N']^T [N'] ds \right] \{X_N^*\} \quad (8)$$

The distributed loading  $\{f^*\}$  can be decomposed into inertial  $\{f_I^*\}$ , gravitational  $\{f_g^*\}$  and aerodynamic drag  $\{f_d^*\}$

$$\{f^*\} = \{f_I^*\} + \{f_g^*\} + \{f_d^*\} \quad (9)$$

where the inertial and gravitational loading are given by

$$\{f_I^*\} = -m \left( \frac{\partial S}{\partial S^*} \right) \{a^*\} \quad (10)$$

$$\{f_g^*\} = mg \left( \frac{\partial S}{\partial S^*} \right) \{a_g\} \quad (11)$$

and the column vector  $\{a_g\} = \{0 \ 0 \ 1\}^T$  for the Z axis aligned with gravity.

The inertial term is next written in terms of the nodal coordinates using (2a) and (7). The resulting inertial (10), gravitational (11) and internal virtual work (8) expressions are then substituted into the statement of the principle of virtual work (4) to give

$$[m]\{\ddot{x}_N^*\} + [c_G]\{\dot{x}_N^*\} + \left[ [k_E] - [k_C] \right] \{x_N^*\} - \{q^*\} = \{g\} + \{r^*\} \quad (12)$$

where the following matrices have been defined:

Consistent Mass

$$[m] = \int_0^L m [N]^T [N] dS \quad (a)$$

Gyroscopic Damping

$$[c_G] = 2 \omega \int_0^L m [N]^T [a_G] [N] dS \quad (b)$$

Elastogeometric Stiffness

$$[k_E] = \frac{1}{2} \int_0^L AE (\{x_N^*\}^T [N']^T [N'] \{x_N^*\} - 1) [N']^T [N'] dS \quad (c)$$

Centripetal Stiffness

$$[k_C] = \omega^2 \int_0^L m [N]^T [a_C] [N] dS \quad (d)$$

Gravitational Equivalent Nodal Loads

$$\{g\} = \int_0^L mg [N]^T [a_G] dS \quad (e)$$

Aerodynamic Drag Equivalent Nodal Loads

$$\{q^*\} = \int_0^L [N]^T \{f_d^*\} dS^* \quad (f)$$

The first five of these were evaluated for a Linear shape function and are given in an earlier paper by the present authors<sup>(9)</sup>.

Since the drag force  $\{f_d^*\}$  is position and velocity dependent, all work with the  $\{q^*\}$  vector is motivated so as to obtain it in terms of damping and stiffness type matrices. The drag force is first decomposed into normal and tangential components

$$\{f_d^*\} = \{f_t^*\} + \{f_n^*\} \quad (14)$$

where

$$\{f_t^*\} = -\frac{1}{2} \rho c_t d^* |v_t^*| \{v_t^*\} \quad (a)$$

$$\{f_n^*\} = -\frac{1}{2} \rho c_n d^* |v_n^*| \{v_n^*\} \quad (b)$$

The tangential and normal drag coefficients are  $c_t$  and  $c_n$ , respectively, the deformed cable diameter  $d^*$ , the density of air  $\rho$ , and the normal and tangential velocity components  $\{v_n^*\}$  and  $\{v_t^*\}$  are

$$\{v_t^*\} = \left( \{v^*\}^T \left\{ \frac{\partial X^*}{\partial S^*} \right\} \right) \left\{ \frac{\partial X^*}{\partial S^*} \right\} \quad (a)$$

(16)

or

$$\{v_t^*\} = \left[ \left\{ \frac{\partial X^*}{\partial S^*} \right\} \left\{ \frac{\partial X^*}{\partial S^*} \right\}^T \right] \{v^*\} \quad (b)$$

and

$$\{v_n^*\} = \{v^*\} - \{v_t^*\} \quad (c)$$

At this time, only the equilibrium configuration will be considered. Assuming small elemental elongations,  $S^*$  can be replaced with  $S$  and  $L^*$  with  $L$ . The equilibrium velocities can then be written in terms of the shape function as

$$\{v\}_0 = \omega [a_G] [N] \{x_N\}_0 \quad (a)$$

$$\{v_t\}_0 = \omega [N'] \{x_N\}_0 \{x_N\}_0^T [N']^T [a_G] [N] \{x_N\}_0 \quad (b) \quad (17)$$

$$\{v_n\}_0 = \omega \left[ [a_G] [N] - [N'] \{x_N\}_0 \{x_N\}_0^T [N']^T [a_G] [N] \right] \{x_N\}_0 \quad (c)$$

where the star superscript has been dropped to indicate the small elongation assumption and the zero subscripts added to denote equilibrium values. Substituting (17) into the expression for the equivalent nodal loads due to aerodynamic drag yields

$$\{q\}_0 = [k_A] \{x_N\}_0 \quad (18)$$

where the aerodynamic stiffness matrix  $[k_A]$  is defined by

$$[k_A] = [k_n^1] + [k_n^2] + [k_t^1] \quad (a) \quad (19)$$

and

$$[k_n^1] = \frac{\omega}{2} \rho c_n d \int_0^L |v_n| [N]^T [a_G] [N] dS$$

$$[k_n^2] = -\frac{\omega}{2} \rho c_n d \left[ \int_0^L |v_n| [N]^T [N'] \{x_N\}_0 \{x_N\}_0^T [N']^T [a_G] [N] dS \right] \quad (b) \quad (20)$$

$$[k_t^1] = \frac{\omega}{2} \rho c_t d \left[ \int_0^L |v_t| [N]^T [N'] \{x_N\}_0 \{x_N\}_0^T [N']^T [a_G] [N] dS \right] \quad (c)$$

The values of  $c_n$ ,  $c_t$ ,  $\rho$  and  $d$  have been assumed constant over the element length. The absolute values of the velocity components are calculated from

$$|v_t| = \left( \{v_t\}^T \{v_t\} \right)^{\frac{1}{2}} \quad (21)$$

$$|v_n| = \left( \{v_n\}^T \{v_n\} \right)^{\frac{1}{2}}$$

These stiffness matrices which are in general not symmetric can be evaluated either using numerical integration or integrated analytically if approximate expressions for the velocity magnitudes are employed.

The equilibrium problem is then defined by

$$[k]\{X_N\}_0 = \{g\} + \{r\} \quad (22)$$

where the element stiffness matrix  $[k]$  is

$$[k] = [k_E] - [k_C] + [k_A] \quad (23)$$

A discrete approximation to the continuous problem may now be found by assembling cable elements in the standard manner. The resultant stiffness matrix is unsymmetric due to the nonconservative nature of aerodynamic drag. The addition of drogue devices at any node is easily accomplished if drogue lift and drag coefficients are known.

### III. Stability

The stability analysis is based on the infinitesimal motion about a given nonlinear equilibrium position. The presence of nonsymmetric terms in the stiffness matrix requires that a dynamic stability analysis be conducted. A convenient way to obtain the linearized dynamic equations is to perform a variation on the equations of motion for a single element and then assemble the total cable system. From (12),

$$[m]\{\ddot{\xi}_N\} + [c_G]\{\dot{\xi}_N\} + \left[ [k_E] - [k_C] + [k_L] \right] \{\xi_N\} + \{\delta q\} = 0 \quad (24)$$

where  $[k_L]$  is the large deflection stiffness matrix found in Henghoid and Russell<sup>(11)</sup> and is given by

$$[k_L] = \int_0^L AE[N']^T[N']\{X_N\}_0\{X_N\}_0^T[N']^T[N']ds \quad (25)$$

and the perturbed motion is  $\{\xi_N\} = \{\delta X_N\}$ .

Evaluating the perturbation of the aerodynamic equivalent nodal loads from (13e), (14), (15) and (16) yields

$$\begin{aligned} \{\delta q\} = & \frac{1}{2} \rho c_n d \int_0^L [N]^T \{v_n\}_0 \delta |v_n| ds + \\ & \frac{1}{2} \rho c_n d \int_0^L |v_n| [N]^T \{\delta v_n\} ds + \\ & \frac{1}{2} \rho c_t d \int_0^L [N]^T \{v_t\}_0 \delta |v_t| ds + \\ & \frac{1}{2} \rho c_t d \int_0^L |v_t| [N]^T \{\delta v_t\} ds \end{aligned} \quad (26)$$

The variations in the absolute velocities are

$$\delta |v_t| = \frac{v_{t0}}{|v_{t0}|} \delta v_t \quad (a)$$

(27)

$$\delta |v_n| = \frac{v_{n0}}{|v_{n0}|} \delta v_n + \frac{v_{t0}}{|v_{n0}|} \delta v_t$$

Other velocity terms needed to evaluate  $\{\delta q\}$  are:

$$\{\delta v\} = [a_T][N]\{\dot{\xi}_N\} + \omega [a_G][N]\{\xi_N\} \quad (a)$$

$$\begin{aligned} v_0 \{\delta v\} = & \omega \{X_N\}_0^T [N]^T [a_G][N]\{\dot{\xi}_N\} + \\ & \omega^2 \{X_N\}_0^T [N]^T [a_C][N]\{\xi_N\} \end{aligned} \quad (b)$$

$$\begin{aligned} \delta v_t = & \{X_N\}_0^T [N']^T [N]\{\dot{\xi}_N\} + \\ & \omega \{X_N\}_0^T [N']^T [a_G][N]\{\xi_N\} + \\ & \omega \{X_N\}_0^T [N]^T [a_G]^T [N']\{\xi_N\} \end{aligned} \quad (c)$$

$$\begin{aligned} \{\delta v_t\} = & \{X_N\}_0^T [N']^T [N']\{X_N\}_0 [N]\{\dot{\xi}_N\} + \\ & \omega [N']\{X_N\}_0 \{X_N\}_0^T [N]^T [a_G]^T [N']\{\xi_N\} + \\ & \omega [N']\{X_N\}_0 \{X_N\}_0^T [N']^T [a_G][N]\{\xi_N\} + \\ & v_{t0} [N']\{\xi_N\} \end{aligned} \quad (d)$$

Substituting the results of (27) and (28) into (26) yields

$$\{\delta q\} = [c_A]\{\dot{\xi}_N\} + [k_A + k_{T_A}]\{\xi_N\} \quad (29)$$

where

$$[c_A] = \sum_{i=1}^6 [c_n^i] + 2[c_t] \quad (a)$$

$$[k_{T_A}] = \sum_{i=1}^{10} [k_n^i] + 2k_t^1 + 2k_t^2 + k_t^3 \quad (b)$$

For clarity, the damping matrices and stiffness matrices are listed in the Appendix. Examination of the damping matrices shows that  $[c_A]$  is symmetric as should be expected.

The perturbed equations of motion for an element can thus be written in the form

$$[m]\{\ddot{\xi}_N\} + [c]\{\dot{\xi}_N\} + [k_T]\{\xi_N\} = \{0\} \quad (31)$$

where

$$[c] = [c_G] + [c_A] \quad (a)$$

$$[k_T] = [k_E] + [k_L] - [k_C] + [k_{T_A}] \quad (b)$$

Defining  $\{\eta_N\}$  as

$$\{\eta_N\} = \begin{Bmatrix} \dot{\xi}_N \\ \xi_N \end{Bmatrix} \quad (33)$$

and assuming exponential motion

$$\{\eta_N\} = \{H_N\} e^{\lambda t} \quad (34)$$

leads to the general eigenvalue formulation

$$[A]\{H_N\} = \lambda[B]\{H_N\} \quad (35)$$

where

$$[A] = \begin{bmatrix} [m] & [0] \\ [0] & -[k_T] \end{bmatrix} \quad [B] = \begin{bmatrix} [0] & [m] \\ [m] & [c] \end{bmatrix} \quad (36)$$

Note the static instability ( $\lambda = 0$ ) is given when the determinant of the tangential stiffness matrix  $[k_T]$  is zero.

#### IV. Solution Procedure

Since the nonlinearity is primarily of a geometrical nature, a Newton-Raphson procedure is used to solve the equilibrium equation (22). A guess is made to initialize the procedure and the resulting equilibrium unbalance  $\{\Psi\}$  calculated from

$$\{\Psi\} = [K]\{x_N\}_0 - \{G\} \quad (37)$$

where  $[K]$  and  $\{G\}$  are the assembled current stiffness matrix and gravitational equivalent nodal load matrix, respectively. A correction to  $\{x_N\}_0$  is then calculated from

$$[K_T]\{dx_N\} = -\{\Psi\}. \quad (38)$$

This procedure is repeated until the maximum normalized increment  $(dx_i/x_i)$  is smaller than an error index  $e_c$ , taken typically, to be .001. Eigenvalues are then calculated from (35) using an eigenvalue subroutine based on the QZ method to determine the system stability.

After equilibrium and stability calculations have been completed for a given rotational frequency, the value of  $W$  can be incremented by  $d\omega$  and a new set of linear equations solved to initialize the iteration procedure at the new frequency. Proceeding in this manner, frequency response curves may be obtained.

The utility of the developed elements will now be demonstrated using the linear element shown in Fig. 2. To verify these elements, theoretical

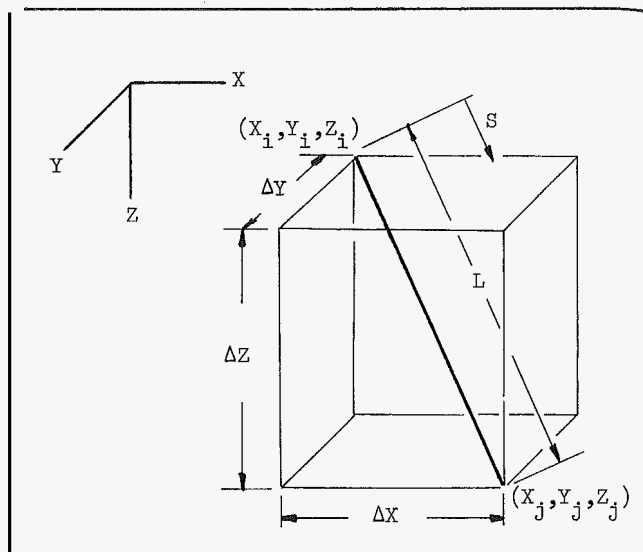


Figure 2. Linear Element

results using approximate expressions for the aerodynamic stiffness, tangential stiffness and damping matrices are compared to results obtained experimentally. All results are presented in non-dimensional form. Spatial coordinates are non-dimensionalized with respect to the unstretched cable length such that the nodal coordinates are given by

$$\{x_N\} = \{x_N\}/l \quad (39)$$

and the tow radius by

$$\epsilon = R_{\text{tow}}/l \quad (40)$$

Other nondimensionalized variables introduced are:

Normal Drag Coefficient

$$\zeta_n = \frac{1}{2} \rho c_n dl/m \quad (41)$$

Tangential Drag Coefficient

$$\zeta_t = \frac{1}{2} \rho c_t dl/m \quad (42)$$

Stiffness to Weight Ratio

$$K = AE/mgl \quad (43)$$

Rotational Frequency

$$\Omega = \omega\sqrt{l/g} \quad (44)$$

The possibility of a spherical drogue at the cable tip has been included. The drogue is characterized by the following two nondimensional parameters:

Drogue Drag Coefficient

$$\zeta_D = 3\rho c_D A_D/l \quad (45)$$

where  $c_D$  is the drogue drag coefficient, considering a drag law in which drag is proportional to the relative velocity squared. The cross-sectional area of the drogue is  $A_D$ .

Drogue to Cable Mass Ratio

$$\mu = M/mg\ell \quad (46)$$

where  $M$  is the drogue mass.

Explicit integration of the aerodynamic stiffness, tangential stiffness and damping matrices is made difficult by the presence of the absolute velocity terms in the integrands. This problem can be overcome either by using numerical integration or by approximating the absolute velocity terms. The second method is used here. The absolute velocities were expanded in a Taylor series in terms of  $\Delta X$ ,  $\Delta Y$  and  $\Delta Z$ , where  $\Delta X$ ,  $\Delta Y$  and  $\Delta Z$  are just the respective differences in the element end points in each direction. The maximum size of any of these is the element length  $L$ . The first two terms were retained in each expansion, these being of order  $L$  and  $L^2$  for the aerodynamic stiffness matrices. This expansion is valid for small element elongations and small element size. Lack of space prevents their reproduction in this report. A complete listing appears in Russell<sup>(12)</sup>.

Equilibrium shapes and their stability are found rather easily and with relatively small computer costs. Overall cable behavior is best described using plots of the three tip parameters - (1) radius  $r_t$ , (2) phase angle  $\phi_t$ , and (3) verticality  $z_t$ , versus rotational frequency  $\Omega$ . The tip radius is measured in a horizontal plane from the axis of rotation to the cable tip.

$$r_t = [(x(1))^2 + (y(1))^2]^{\frac{1}{2}} \quad (47)$$

The phase angle is used to measure the lag of the tip from the tow point and is given by

$$\phi_t = \arctan (y(1)/x(1)) \quad (48)$$

while the verticality is simply the tip value of  $z$

$$z_t = z(1) \quad (49)$$

where all quantities have been defined in non-dimensional form.

Typical results for three values of drag are sketched in Fig. 3. A hardening spring character is observed with the tow radius  $\epsilon$  playing the role of the magnitude of the excitation.

For low drag (M), the system behavior is similar to that of the system without drag. For moderate values of drag (ME), jump phenomena are possible, near the system's first resonant frequency. Also for moderate (ME) and high (HI) values of drag, a detached branch of the equilibrium curve appears in the upper right of the figure. A dynamic stability analysis shows that the dashed portions of the curve are statically unstable, while the dotted portions of the curves are dynamically unstable. The qualitative behavior of these solutions and their stability has been confirmed in a related experiment, Russell<sup>(12)</sup>.

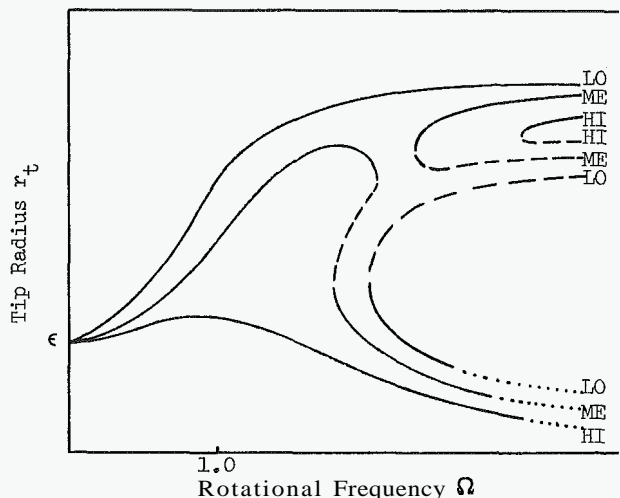


Figure 3. Sketch of Typical Equilibrium Solutions

A typical set of experimental results for a tow radius of 9 inches and cable length of 25.75 inches is used to confirm the theory. The experimental cable model was .0185 inch diameter silk thread weighing  $4.519 \times 10^{-5}$  lb/ft. A spherical drogue with mean diameter of .148 inch weighing  $9.921 \times 10^{-5}$  lb was attached to the cable tip. Normal and tangential drag coefficients for a smooth cylinder were used;  $c_n = 1.2$ , and  $c_t = 0.01$ . The drag coefficient for the drogue was taken as that of a sphere,  $c_D = 0.47$ . Experimental results for tip radius and verticality are shown in Figs. 4 and 5. No experimental phase angle data was obtained.

Theoretical results were obtained using a nine-element cable discretization with the experimental cable parameters. These results are shown in Figs. 4, 5 and 6. Since no experimental value of  $K$  was measured, a value of 1000 was used in the theoretical calculations. Results indicate relative insensitivity to this parameter except for large tip radii and high rotational frequencies.

Theoretical equilibrium results are, in general, in very good agreement with those obtained experimentally. The only region where the results disagree is near the jump from large tip radius to small, the theoretical jump occurring sooner than the actual. Since drag is most important in this region, any differences in theoretical and actual drag coefficients would produce the greatest differences in theoretical and experimental results here. Thus, the discrepancy is explained on the basis of an underestimation of the actual drag caused by not taking the rough surface of the thread into account.

The stability analysis confirms the zero eigenvalues at the large-to-small and small-to-large radius jumps. The dynamic instability was predicted at  $\Omega = 3.08$ , while it actually occurred

at  $\Omega = 3.70$ . The discrepancy once more is explained on underestimation of the drag. Since only the first two eigenvalues were of interest, the nine nodes of the static analysis were condensed to three for the dynamic analysis. No attempt was made to obtain equilibrium solutions in the statically unstable region. Although no upper bound of the unstable region was found for  $\Omega < 7.0$  in this case, the bounded behavior has been established for other cases, both experimentally and theoretically.

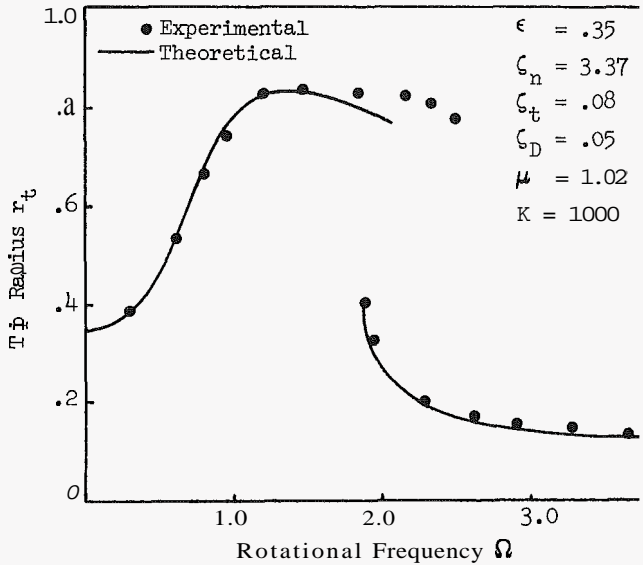


Figure 4. Frequency Response

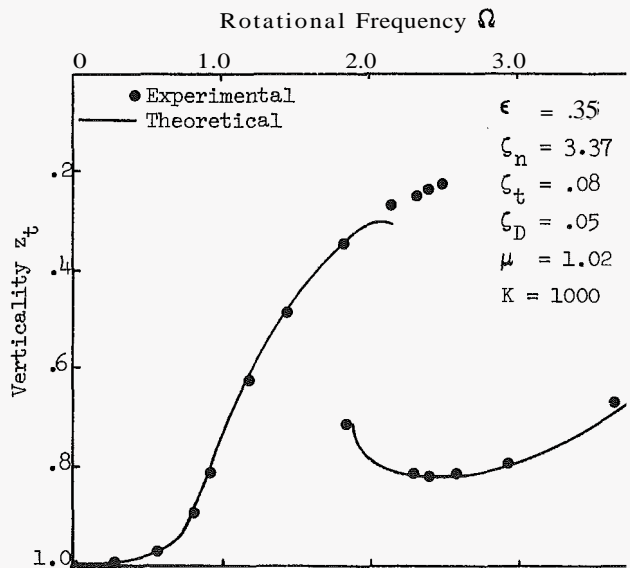


Figure 5. Verticality

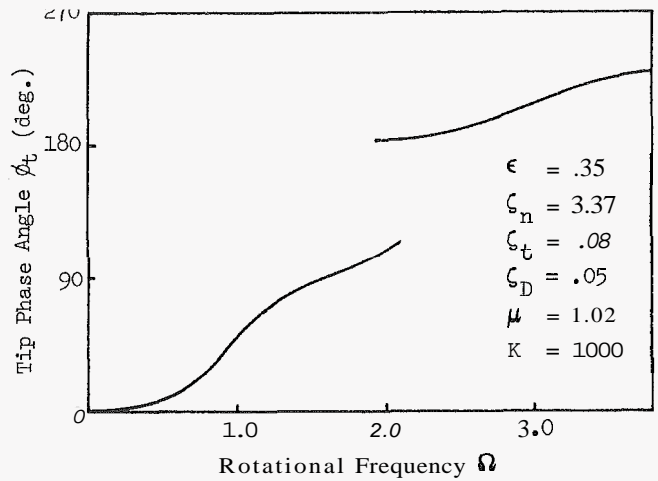


Figure 6. Phase Angle

## VI. Conclusions

A finite element representation of aerodynamic drag acting on a whirling cable has been accomplished. This representation places the position dependent drag forces in terms of stiffness matrices referred to a rotating reference frame, thus allowing equilibrium solutions to be obtained in the rotating frame. Position dependent tangential stiffness and damping matrices are used in the perturbed equations of motion. Gravitational, centripetal acceleration, coriolis and elastic effects are also included in the element. Large cable rotations and position dependent forces created by the velocity squared drag laws cause the problem to be highly nonlinear.

A computer program has been written for the single whirling cable with a spherical drogue attached to the cable tip. This program has proven to be efficient and capable of coping with multi-valued solutions. The Newton-Raphson method is used to find equilibrium positions and a dynamic perturbation is used to determine the stability of each solution. Modification of the program to solve related problems such as the whirling cable attached at both ends and lasso problem is easily accomplished.

Physical phenomena encountered for the whirling cable include static and dynamic instabilities, jumps from one equilibrium configuration to another, and detached solution branches. The static instabilities and jumps are typical of those observed in damped, hardening, nonlinear, spring-mass systems. The dynamic instability is peculiar to nonconservative systems, while the detached branches are rarely seen in the frequency response of mechanical systems. Space has not allowed a study of the effects of the various problem parameters on these phenomena to be included, but a later paper will concentrate on this area.

This paper concentrates on the mathematical development of the aerodynamic portion of a whirling cable element and the solution of a seemingly simply assembly, a single whirling cable. Theoretical results obtained agree with those obtained

experimentally. The richness of solutions and associated stability phenomena makes it a fascinating study and impossible to document completely here.

### Appendix

The perturbed element aerodynamic damping and stiffness matrices defined in (30) are given below:

#### Aerodynamic Damping Matrices

$$[c_n^1] = \frac{\omega^2 \rho c_n d}{2} \left[ \int_0^L \frac{1}{|v_{n0}|} [N]^T [a_G] [N] \{X_N\}_0 \{X_N\}_0^T [N]^T [a_G]^T [N] ds \right] \quad (a)$$

$$[c_n^2] = \frac{-\omega \rho c_n d}{2} \left[ \int_0^L \frac{v_{t0}}{|v_{n0}|} [N]^T [a_G] [N] \{X_N\}_0 \{X_N\}_0^T [N']^T [N] ds \right] \quad (b)$$

$$[c_n^3] = \frac{\omega \rho c_n d}{2} \left[ \int_0^L \frac{v_{t0}}{|v_{n0}|} [N]^T [N'] \{X_N\}_0 \{X_N\}_0^T [N]^T [a_G]^T [N] ds \right] \quad (c)$$

$$[c_n^4] = \frac{\rho c_n d}{2} \left[ \int_0^L \frac{(v_{t0})^2}{|v_{n0}|} [N]^T [N'] \{X_N\}_0 \{X_N\}_0^T [N']^T [N] ds \right] \quad (d)$$

$$[c_n^5] = \frac{\rho c_n d}{2} \int_0^L |v_{n0}| [N]^T [N] ds \quad (e)$$

$$[c_n^6] = \frac{-\rho c_n d}{2} \left[ \int_0^L |v_{n0}| [N]^T [N'] \{X_N\}_0 \{X_N\}_0^T [N']^T [N] ds \right] \quad (f)$$

$$[c_t] = \frac{\rho c_t d}{2} \left[ \int_0^L |v_{t0}| [N]^T [N'] \{X_N\}_0 \{X_N\}_0^T [N']^T [N] ds \right] \quad (g)$$

#### Aerodynamic Tangential Stiffness Matrices

$$[k_n^3] = \frac{\omega^3 \rho c_n d}{2} \left[ \int_0^L \frac{1}{|v_{n0}|} [N]^T [a_C] [N] \{X_N\}_0 \{X_N\}_0^T [N]^T [a_C]^T [N] ds \right] \quad (a)$$

$$[k_n^4] = \frac{-\omega^2 \rho c_n d}{2} \left[ \int_0^L \frac{v_{t0}}{|v_{n0}|} [N]^T [a_G] [N] \{X_N\}_0 \{X_N\}_0^T [N]^T [a_G]^T [N'] ds \right] \quad (b)$$

$$[k_n^5] = \frac{-\omega^2 \rho c_n d}{2} \left[ \int_0^L \frac{v_{t0}}{|v_{n0}|} [N]^T [a_G] [N] \{X_N\}_0 \{X_N\}_0^T [N']^T [a_G]^T [N] ds \right] \quad (c)$$

$$[k_n^6] = \frac{-\omega \rho c_n d}{2} \left[ \int_0^L v_{t0} [N]^T [N'] \{X_N\}_0 \{X_N\}_0^T [N]^T [a_C]^T [N] ds \right] \quad (d)$$

$$[k_n^7] = \frac{\rho c_n d}{2} \left[ \int_0^L (v_{t0})^2 [N]^T [N'] \{X_N\}_0 \{X_N\}_0^T [N]^T [a_G]^T [N'] ds \right] \quad (e)$$

$$[k_n^8] = \frac{\rho c_n d}{2} \left[ \int_0^L (v_{t0})^2 [N]^T [N'] \{X_N\}_0 \{X_N\}_0^T [N']^T [a_G]^T [N] ds \right] \quad (f) \quad (A2)$$

$$[k_n^9] = \frac{-\omega \rho c_n d}{2} \left[ \int_0^L |v_{n0}| [N]^T [N'] \{X_N\}_0 \{X_N\}_0^T [N]^T [a_G]^T [N'] ds \right] \quad (g)$$

$$[k_n^{10}] = \frac{\rho c_n d}{2} \int_0^L v_{t0} |v_{n0}| [N]^T [N'] ds \quad (h)$$

$$[k_t^2] = \frac{\rho c_t d}{2} \left[ \int_0^L |v_{t0}| [N]^T [N'] \{X_N\}_0 \{X_N\}_0^T [N']^T [a_G]^T [N'] ds \right] \quad (i)$$

$$[k_t^3] = \frac{\rho c_t d}{2} \int_0^L (v_{t0})^2 [N]^T [N'] ds \quad (j)$$

### References

- 1) Kolodner, I.I., "Heavy Rotating String -- A Nonlinear Eigenvalue Problem," Communications on Pure and Applied Mathematics, Vol. VIII, 1955, pp. 334-338.
- 2) Wu, C.H., "Whirling of a String at Large Angular Speeds -- A Nonlinear Eigenvalue Problem with Moving Boundary Layers," SIAM Journal of Applied Mathematics, Vol. 22, No. 1, Jan. 1972, pp. 1-13.
- 3) Caughey, T.K., "Whirling of a Heavy Chain," Proceedings of the Third U.S. National Congress of Applied Mechanics, 1958, pp. 61-108.
- 4) Skop, R. A., and Choo, Y., "The Configuration of a Cable Towed in a Circular Path," Journal of Aircraft, Vol. 8, No. 11, Nov. 1971, pp. 856-862.

- 5) Crist, S.A., "Analysis of the Motion of a Long Wire Towed from an Orbiting Aircraft," The Shock and Vibration Bulletin, Bulletin 41, Dec. 1970, pp. 61-73.
- 6) Crist, S.A., "Steady State Shape of Orbiting Trailing Wire System," United States Air Force Academy Research Report, No. 72-8, Oct. 1972.
- 7) Huang, J., "Mathematical Model for Long Cable Towed by Orbiting Aircraft," U.S. Naval Air Development Center Report NADC-AM-6849, June 1969.
- 8) Choo, Y., "Analytical Investigation of the Three-Dimensional Motion of Towed Systems," W.D. Dissertation, The Catholic University of America, June 1970.
- 9) Russell, J.J. and Anderson, W.J., "Whirling Cable Subjected to Viscous Drag," Proceedings of the 1974 International Conference on Finite Element Methods in Engineering, The University of New South Wales, pp. 661-676.
- 10) Webster, R.L., "Structural Response of Arbitrary Underwater Cable Systems," Ocean Engineering Mechanics, OED - Vol. 1, ASME, New York, 1975, pp. 43-59.
- 11) Henghold, W.M. and Russell, J.J., "Equilibrium and Natural Frequencies of Cable Structures (A Nonlinear Finite Element Approach)," Proceedings of the Second National Symposium on Computerized Structural Analysis and Design, Mar. 1976.
- 12) Russell, J.J., "Equilibrium and Stability of a Whirling Cable," W.D. Dissertation, The University of Michigan, 1974.